EMBO reports

scientific report

Bacterial Na^+-ATP synthase has an undecameric rotor

Henning Stahlberg[1], Daniel J. Müller[1,2], Kitaru Suda[1], Dimitrios Fotiadis[1], Andreas Engel[1,+], Thomas Meier[3], Ulrich Matthey[3] & Peter Dimroth[3]

[1]M.E. Müller Institute for Structural Biology, Biozentrum, University of Basel, Klingelbergstrasse 70, CH-4056 Basel, [3]Institute of Microbiology, ETH, Schmelzbergstrasse 7, CH-8092 Zürich, Switzerland and [2]Max-Planck-Institute of Molecular Cell Biology and Genetics, Pfotenhauerstrasse 108, D-01307 Dresden, Germany

Received December 4, 2000; revised January 11, 2001; accepted January 15, 2001

Synthesis of adenosine triphosphate (ATP) by the F_1F_0 ATP synthase involves a membrane-embedded rotary engine, the F_0 domain, which drives the extra-membranous catalytic F_1 domain. The F_0 domain consists of subunits a_1b_2 and a cylindrical rotor assembled from 9–14 α-helical hairpin-shaped *c*-subunits. According to structural analyses, rotors contain 10 *c*-subunits in yeast and 14 in chloroplast ATP synthases. We determined the rotor stoichiometry of *Ilyobacter tartaricus* ATP synthase by atomic force microscopy and cryo-electron microscopy, and show the cylindrical sodium-driven rotor to comprise 11 *c*-subunits.

INTRODUCTION

In most forms of life, ATP synthesis is driven by a transmembrane electrochemical gradient, generated by light or oxidative reactions. The flow of protons or sodium ions down the gradient propels the smallest existing rotary motor, the membrane resident F_0 part of the ATP synthase. Rotation of the 5–7 nm large cylindrical *c*-oligomer in F_0 is transmitted to a long rod (Gibbons *et al.*, 2000), which induces the conformational changes required for production of ATP in the globular extra-membranous F_1 part of the enzyme. The latter exhibits a highly conserved structure comprising three catalytic sites arranged around a 3-fold axis (Abrahams *et al.*, 1994), which strongly suggests that three ATPs are synthesized for each full rotation of the long rod. Therefore, the proton/ATP ratio appears to be directly linked to the stoichiometry of the rotor, which is thought to rotate by $2\pi/n$ per translocated cation, where n is the number of *c*-subunits in the ring. Since such central processes have been tuned to maximum performance during evolution, variation in the ring stoichiometry (n = 10 in yeast mitochondria and n = 14 in spinach chloroplasts) came as a surprise.

Much uncertainty surrounds the proton/ATP ratio. Early results suggested a value of two for mitochondria, where the situation is complicated by the transport systems for ADP, P_i and ATP. Currently four protons/ATP is the accepted overall value for mitochondria (Ferguson, 2000) as well as chloroplasts (Van Walraven *et al.*, 1996; Pänke and Rumberg, 1997). The prediction of 12 *c*-subunits in the F_0 ring in *Escherichia coli*, based on genetic fusion of *c*-subunits and cross-linking experiments (Jones and Fillingame, 1998), is in perfect agreement with this proton/ATP ratio (12 protons would cause a 360° rotation of the *c*-ring and release three ATP molecules from F_1). Therefore, other stoichiometries for the rotary motor from different sources appeared to be counterintuitive. A recent discussion sheds light on the puzzle: even if the overall proton/ATP ratio is close to four, approximately three protons are available per ATP in mitochondria, because one proton is consumed during the transport of ATP into the cytosol and the transport of ADP as well as P_i back into the mitochondrial matrix (Ferguson, 2000). The values, calculated from the ring stoichiometries, are 3.3 protons/ATP in mitochondria (Stock *et al.*, 1999) and 4.7 protons/ATP in chloroplasts (Seelert *et al.*, 2000). Although the latter value is significantly higher than recent experimental results (Pänke and Rumberg, 1997), the suggested relative proton translocation stoichiometry of 3:4 in mitochondria versus chloroplasts (Ferguson, 2000) is quite close to the relative number of subunits per ring, 10:14. However, accurate measurements of the mitochondrial P:O ratio when electrons pass from NADH to oxygen (P:O ≥2.5) set an upper limit for the proton/ATP ratio of four, provided that this oxidative process translocates 10 protons outwards as

+Corresponding author. Tel: +41 61 267 2262; Fax: +41 61 267 2109; E-mail: Andreas.Engel@unibas.ch

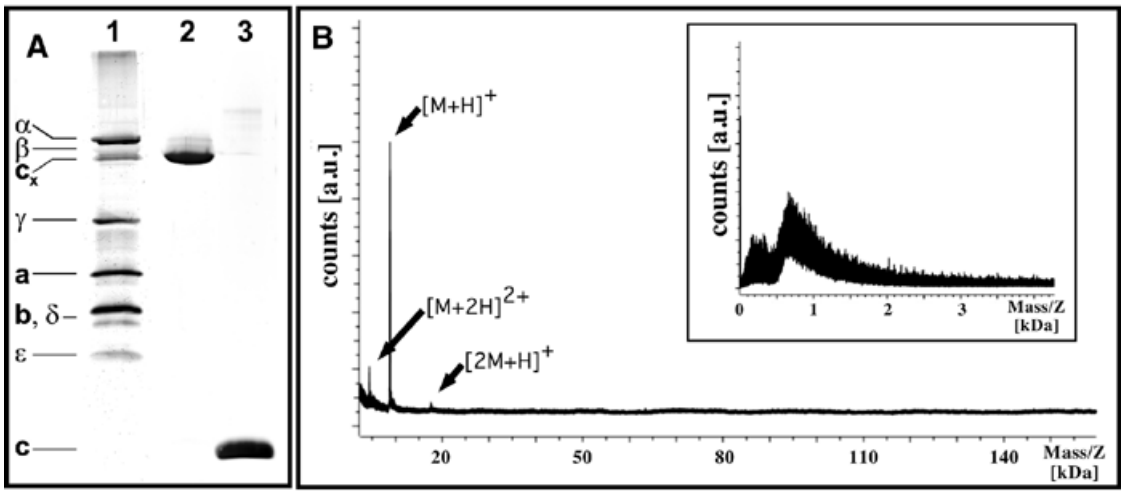

Fig. 1. (**A**) Purification of ATP synthase from *I. tartaricus*. Lane 1, silver-stained SDS–PAGE of ATP synthase; lane 2, purified subunit c_x-oligomer, running below the β-subunit (52 kDa; Neumann *et al.*, 1998) due to strong hydrophobicity; lane 3, subunit *c*-monomer derived from the oligomer by acidification with trichloroacetic acid. (**B**) MALDI spectrum showing a prominent peak at 8790 ± 5 Da, corresponding to the mono-ionized *c*-monomer $[M + H]^+$. Further peaks can be assigned to the double-ionized monomer $[M + 2H]^{2+}$ and the mono-ionized *c*-dimer $[2M + H]^+$. Additional masses were not detected, neither at higher masses up to 140 kDa, nor below 4 kDa (insert).

commonly accepted (Ferguson, 2000). The most precise proton/ATP ratios currently available are based on structural investigations. These data, however, do not provide clues about the restrictions that apply for the number of *c*-subunits to assemble into functional rotors in different organisms. We have, therefore, elucidated the stoichiometry of the *c*-oligomer of the Na^+-ATPase of *Ilyobacter tartaricus*, presenting for the first time data for a prokaryotic organism and for a sodium-dependent ATP synthase.

RESULTS

Protein purification and crystallization

Sodium ions propel the rotary motor of the ATP synthase from *I. tartaricus* by a mechanism that is similar to the proton movement and torque generation in *E. coli* ATP synthase (Junge *et al.*, 1997; Elston *et al.*, 1998; Dimroth *et al.*, 1999). The sodium-translocating ATP synthase of *I. tartaricus* is one of a few examples comprising c_x-oligomers of extreme stability (Neumann *et al.*, 1998). This enabled us to isolate the pure c_x-oligomer, which moves on SDS–PAGE exactly as c_x in the purified ATP synthase (Figure 1A, lanes 1 and 2). Such behaviour is similar to that of ring-shaped oligomers of chloroplast subunit III (Seelert *et al.*, 2000). After acidification, c_x dissociates completely into monomers (Figure 1A, lane 3). Upon reconstitution of c_x-oligomers into lipid bilayers at a low lipid-to-protein ratio, rings assembled into two-dimensional (2D) crystalline arrays. Matrix-assisted laser desorption ionization (MALDI) mass spectrometry of such samples yields a single monomeric mass of 8790 ± 5 Da (Figure 1B), corresponding well with the calculated monoisotopic mass of 8790.71 Da for subunit *c* (our unpublished data). Two additional signals can be assigned to *c*-dimers and double-charged *c*-monomers. No additional masses were detected (Figure 1B), documenting that subunit *c* is the only protein present in the crystals.

Atomic force microscopy

Atomic force microscopy (AFM) (Müller *et al.*, 1997, 1999) reveals loosely packed disordered membranes and highly ordered crystalline arrays (Figure 2A). The thickness of the latter is 10.5 ± 0.4 nm, whereas that of the surrounding lipid bilayer is 4.1 ± 0.3 nm. Higher magnification scans show a crystalline arrangement of ring-like c_x-oligomers, with adjacent rotors having different heights (Figure 2B). This suggests that they are oppositely oriented within the bilayer, analogous to the crystalline packing arrangement of the subunit III rings of chloroplast ATP synthase (Seelert *et al.*, 2000). Thus, both the cytoplasmic surface and the extracellular surface of the c_x-oligomer were imaged in one topograph. Since the higher ends of the c_x complexes protrude by 1.0 ± 0.2 nm above the lower ends, the AFM stylus cannot resolve the subunits of the lower rings (Figure 2B). However, densely packed, non-crystalline patches allowed the lower ends to be contoured with the stylus at high resolution (Figure 2C). As seen directly in unprocessed AFM topographs, individual rotors with low ends have 11 subunits (Figure 2D), whereas the subunits of c_x complexes exposing their higher end are not resolved (Figure 2E). Therefore, individual rotors with high or low ends were selected, aligned, classified and averaged, revealing the 11-fold symmetry of the c_x-oligomers (Figure 2F and G). The lower end protrudes 1.5 ± 0.3 nm from the bilayer and shows a central depression with a diameter of 1.5 ± 0.3 nm (Figure 2F). In contrast, the higher end exhibits a central plug that is 0.7 ± 0.3 nm higher than the ring, which itself protrudes 2.5 ± 0.3 nm from the bilayer (Figure 2G).

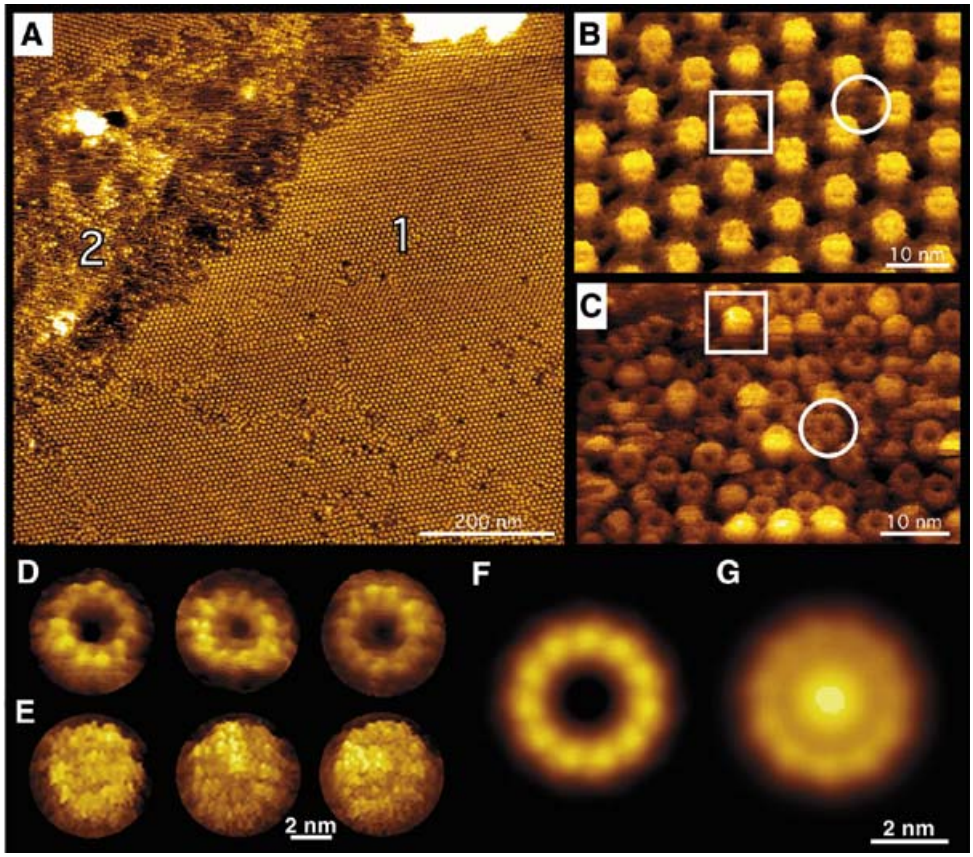

Fig. 2. AFM topographs of reconstituted c_x-oligomers from ATP synthase of *I. tartaricus*. (**A**) Overview showing a 2D crystal of more than 2 μm diameter (1) next to a densely packed region (2). (**B**) The crystalline area is organized in a hexagonal head-to-tail packing. The higher ends (square) of the c_x-oligomers are well resolved, whereas the AFM stylus cannot effectively image the lower ends (circle). (**C**) The densely packed area as in (A, 2) allows the imaging of the lower ends of the c_x-oligomers. (**D**) AFM topographs of individual lower rings and (**E**) of the higher rings. (**F**) Average of 172 lower rings as in (D) showing a right-handed vorticity. (**G**) Average of 145 higher rings as in (E) showing a left-handed vorticity. The higher rings exhibit central plugs. The outer diameter of the higher rings was 5.4 ± 0.3 nm and the lower rings was 5.7 ± 0.3 nm. These values are slightly larger than those determined by electron microscopy due to the AFM tip geometry.

Transmission cryo-electron microscopy

Transmission cryo-electron microscopy (cryo-EM; Dubochet *et al.*, 1988; Henderson *et al.*, 1990) documents the order of the 2D crystals (Figure 3A). The non-symmetrized projection structure (symmetry group P1) at 6.9 Å resolution (Figure 3B; Table I) shows a pseudo-hexagonal arrangement of ring-like structures with 11 subunits. The rings have an outer diameter of 5.0 ± 0.2 nm and an inner diameter of 1.7 ± 0.2 nm. This outer diameter is slightly larger than that of the c_{10}-complexes of yeast ATP synthase, but is smaller than that measured for the rotor of the chloroplast ATP synthase comprising 14 subunits. Each subunit of the 11-fold symmetrized projection map (Figure 3C) exhibits two densities with a slight vorticity, which is also visible in the averaged AFM topographs (Figure 2F and G), resembling the arrangement of the two α-helices of subunit *c* of the yeast ATP synthase (Stock *et al.*, 1999). The cryo-EM projection map (Figure 3B) shows a much lower density in the interior of the rings than for the surrounding lipid bilayer. This implies that the plug observed in the AFM topographs (Figure 2D) is of a lower molecular weight than a lipid bilayer. As shown by biochemical analyses (Figure 1), no additional protein is present in the 2D crystals. This indicates that the central protrusion represents either a part of the *c*-subunit, or a monolayer of lipids, consistent with the density observed in the central cavity of the yeast ATP synthase *c*-oligomer (Stock *et al.*, 1999).

DISCUSSION

The structural data presented here are from isolated c_x-oligomers that had the same molecular mass as in the complete F_1F_0-ATP synthase and that remained intact during the course of the sample preparation (Figure 1A, lanes 1–3). The undecameric state of the *c*-oligomer is documented by AFM and by electron crystallography; invariably, all *c*-subunit rings observed exhibited the c_{11} stoichiometry. According to this observation and the extreme stability of the *c*-subunit ring, our results likely reflect the native structure of this assembly. The novel *c*-oligomer stoichiometry is the first determined for a prokaryotic organism and represents the first analysis for a sodium-powered ATP synthase.

None of the *c*-subunit assemblies studied so far by structural methods exhibits a stoichiometry that can be divided by three. A symmetry mismatch is expected to facilitate the rotary mechanism (Stock *et al.*, 2000; see also Simpson *et al.*, 2000). It also

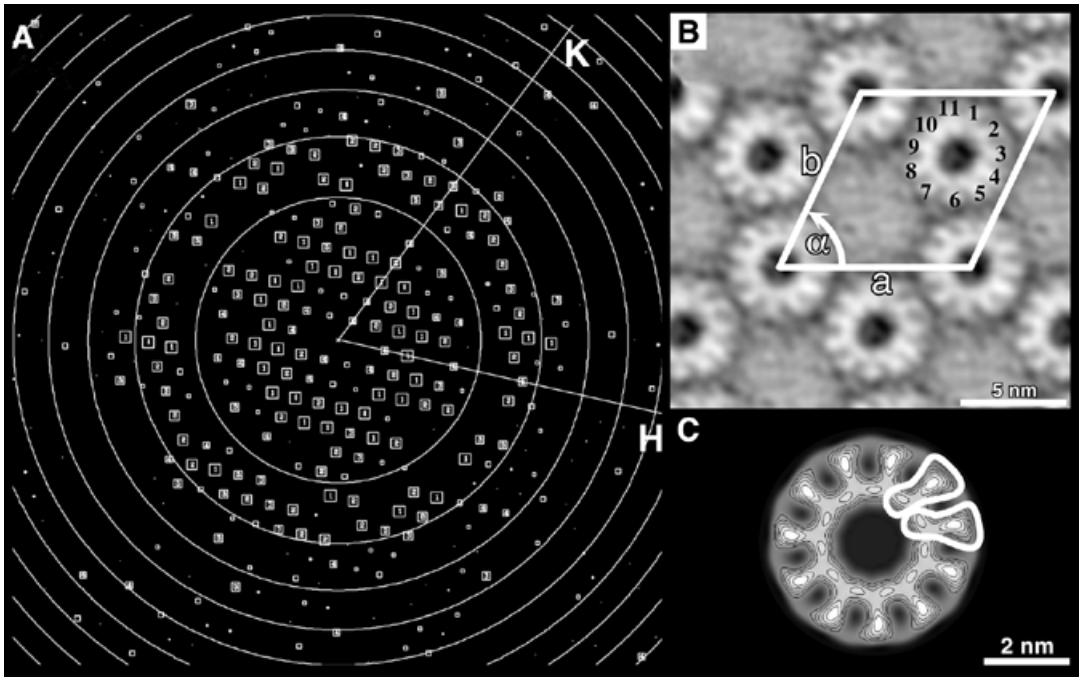

Fig. 3. Cryo-EM imaging of the 2D crystals. (**A**) The calculated IQ plot after lattice-unbending documents the quality of the 2D crystals. The border of the plot is at 6.0 Å. (**B**) The non-symmetrized projection map (space group P1) was calculated at 6.9 Å resolution, showing a pseudo-hexagonal arrangement of the 11-fold symmetric rings. The unit cell comprises two rings; the cell dimensions are $a = 8.9 \pm 0.2$ nm, $b = 9.1 \pm 0.2$ nm and $\alpha = 65° \pm 1°$. (**C**) Symmetrized c_x-oligomers, showing densities of transmembrane α-helices. The two oppositely oriented rings of a unit cell in the map in (B) at 6.9 Å resolution were windowed and one of them was mirrored to obtain the same sidedness. Subsequent averaging and 11-fold symmetrization resulted in the reproduced projection structure. Proposed locations for two *c*-monomers are indicated.

Table I. Phase residuals in resolution ranges (random = 90°)

Resolution (Å)		IQ value (signal/noise ~8/IQ)[a]								IQ-weighted residuals
from	to	1	2	3	4	5	6	7	8	
100.0	13.8	9.4	24.9	21.8	22.5	29.8	17.4	24.6	73.1	17.5
		27	15	15	9	7	7	2	8	90
13.8	9.8	19.8	19.5	28.0	44.5	75.0	33.9	31.9	86.9	24.2
		9	25	7	2	5	3	3	6	60
9.8	8.0	7.6	19.5	24.4	32.4	27.1	62.3	69.8	58.1	28.1
		4	10	12	7	10	10	6	19	78
8.0	6.9	0.0	0.0	3.4	56.9	48.8	40.7	35.3	65.4	40.3
		0	0	1	2	3	4	2	16	28
6.9	6.2	0.0	0.0	61.8	48.9	54.6	22.4	56.4	79.1	54.5
		0	0	3	2	2	1	3	17	28

[a]Spots are classified according to Henderson *et al.* (1986). Phase residuals (in degrees, top lines) during merging and the numbers of spots

implicates an elastic connection between F_1 and F_0 ATP synthase, possibly the γ-subunit (W. Junge, personal communication; Cherepanov *et al.*, 1999; Feniouk *et al.*, 1999). While for yeast mitochondria, which need one proton for ATP translocation, a value of three protons/ATP for the ATP synthase is expected from biochemical measurements (Ferguson, 2000), similar experiments gave a value of four protons/ATP in chloroplasts (Van Walraven *et al.*, 1996; Pänke and Rumberg, 1997). This varying ratio might be correlated with different ion motive forces that drive the enzymes in the different organisms. Although slightly larger, the structurally determined values of 3.3 for yeast and 4.7 for chloroplasts are compatible with these biochemical measurements. No biochemical data are available to be compared with the newly determined stoichiometry for the

I. tartaricus ATP synthase of 3.7 sodium ions/ATP. Further structural analyses at the atomic level and accurate measurements of the cation/ATP ratio are now required to improve our understanding of the smallest existing rotary motors.

METHODS

Purification and 2D crystallization. ATP synthase from *I. tartaricus* was purified as described (Neumann *et al.*, 1998). c_x-oligomers were purified from disrupted ATP synthase complexes by sucrose density gradient centrifugation to a final concentration of 0.8 mg/ml. For crystallization c_x-oligomers solubilized in 2.4% β-octyl-glucoside were mixed with palmitoyl-oleoyl phosphatidylcholine (POPC) at a lipid-to-protein ratio of 1.5 (w/w), and dialysed in a temperature-controlled dialysis apparatus for 60 h against detergent-free buffer (200 mM NaCl, 10 mM Tris–HCl pH 7.0).

Atomic force microscopy. The samples were diluted to a concentration of ~10 µg/ml in 300 mM KCl, 10 mM Tris–HCl pH 7.8 and adsorbed to freshly cleaved mica. Contact mode AFM topographs were recorded in the same buffer, at room temperature, at a stylus loading force of <100 pN and a line frequency of typically 4–6 Hz. The AFM used was a Nanoscope III (Digital Instruments, Santa Barbara, CA) equipped with a *J*-scanner (scan size 120 µm) and a fluid cell. Cantilevers (Olympus, Tokyo, Japan) had oxide-sharpened Si_3N_4 tips and a spring constant of 0.09 N/m. No differences between topographs recorded simultaneously in trace and in re-trace direction were observed, indicating that the scanning process did not influence the appearance of the biological sample. Three-dimensional surface structures of the AFM topographs are displayed in a perspective view (5° tilt).

Cryo-electron microscopy. The 2D crystals were embedded in 1% trehalose on carbon-coated copper grids. Grids were blotted, quick-frozen and transferred with a Gatan 626 cryo holder into a Hitachi H8000 transmission electron microscope, operated at 200 kV. Images were recorded at a nominal magnification of 50 000× on Kodak SO 163 film, applying low-dose conditions (5 $e^-/Å^2$). Digitized negatives were processed with the MRC program suite (Henderson *et al.*, 1990). Amplitudes and phases from two images were corrected for the contrast transfer function and merged.

ACKNOWLEDGEMENTS

We thank Wolfgang Junge, Karl-Heinz Altendorf, Nathan Nelson and Norbert Dencher for critical reading of the manuscript. We thank Paul Jenoe for the possibility of using the mass spectrometer. The work was supported by Swiss National Foundation for Scientific Research and the M.E. Müller Foundation of Switzerland.

REFERENCES

Abrahams, J.P., Leslie, A.G., Lutter, R. and Walker, J.E. (1994) Structure at 2.8 Å resolution of F_1-ATPase from bovine heart mitochondria. *Nature*, **370**, 621–628.

Cherepanov, D.A., Mulkidjanian, A.Y. and Junge, W. (1999) Transient accumulation of elastic energy in proton translocating ATP synthase. *FEBS Lett.*, **449**, 1–6.

Dimroth, P., Wang, H., Grabe, M. and Oster, G. (1999) Energy transduction in the sodium F-ATPase of *Propionigenium modestum*. *Proc. Natl Acad. Sci. USA*, **96**, 4924–4929.

Dubochet, J., Adrian, M., Chang, J.-J., Homo, J.-C., Lepault, J., McDowall, A.W. and Schultz, P. (1988) Cryo-electron microscopy of vitrified specimens. *Q. Rev. Biophys.*, **21**, 129–228.

Elston, T., Wang, H. and Oster, G. (1998) Energy transduction in ATP synthase. *Nature*, **391**, 510–513.

Feniouk, B.A., Cherepanov, D.A., Junge, W. and Mulkidjanian, A.Y. (1999) ATP-synthase of *Rhodobacter capsulatus*: coupling of proton flow through F_0 to reactions in F_1 under the ATP synthesis and slip conditions. *FEBS Lett.*, **445**, 409–414.

Ferguson, S.J. (2000) ATP synthase: what dictates the size of a ring? *Curr. Biol.*, **10**, R804–R808.

Gibbons, C., Montgomery, M.G., Leslie, A.G. and Walker, J.E. (2000) The structure of the central stalk in bovine F_1-ATPase at 2.4 Å resolution. *Nature Struct. Biol.*, **7**, 1055–1061.

Henderson, R., Baldwin, J.M., Downing, K.H., Lepault, J. and Zemlin, F. (1986) Structure of purple membrane from *Halobacterium halobium*: recording, measurement and evaluation of electron micrographs at 3.5 Å resolution. *Ultramicroscopy*, **19**, 147–178.

Henderson, R., Baldwin, J.M., Ceska, T.A., Zemlin, F., Beckmann, E. and Downing, K.H. (1990) Model for the structure of bacteriorhodopsin based on high-resolution electron cryo-microscopy. *J. Mol. Biol.*, **213**, 899–929.

Jones, P.C. and Fillingame, R.H. (1998) Genetic fusions of subunit *c* in the F_o sector of H^+-transporting ATP synthase. *J. Biol. Chem.*, **273**, 29701–29705.

Junge, W., Lill, H. and Engelbrecht, S. (1997) ATP synthase: an electrochemical transducer with rotatory mechanics. *Trends Biochem. Sci.*, **22**, 420–423.

Müller, D.J., Amrein, M. and Engel, A. (1997) Adsorption of biological molecules to a solid support for scanning probe microscopy. *J. Struct. Biol.*, **119**, 172–188.

Müller, D.J., Fotiadis, D., Scheuring, S., Müller, S.A. and Engel, A. (1999) Electrostatically balanced subnanometer imaging of biological specimens by atomic force microscopy. *Biophys. J.*, **76**, 1101–1111.

Neumann, S., Matthey, U., Kaim, G. and Dimroth, P. (1998) Purification and properties of the F_1F_0 ATPase of *Ilyobacter tartaricus*, a sodium ion pump. *J. Bacteriol.*, **180**, 3312–3316.

Pänke, O. and Rumberg, B. (1997) Energy and entropy balance of ATP synthesis. *Biochim. Biophys. Acta*, **1322**, 183–194.

Seelert, H., Poetsch, A., Dencher, N.A., Engel, A., Stahlberg, H. and Müller, D.J. (2000) Imaging the proton powered motor of chloroplast ATP synthase. *Nature*, **405**, 418–419.

Simpson, A.A. *et al.* (2000) Structure of the bacteriophage ϕ29 DNA packaging motor. *Nature*, **408**, 745–750.

Stock, D., Leslie, A.G. and Walker, J.E. (1999) Molecular architecture of the rotary motor in ATP synthase. *Science*, **286**, 1700–1705.

Stock, D., Gibbons, C., Arechaga, I., Leslie, A.G. and Walker, J.E. (2000) The rotary mechanism of ATP synthase. *Curr. Opin. Struct. Biol.*, **10**, 672–679.

Van Walraven, H.S., Strotmann, H., Schwarz, O. and Rumberg, B. (1996) The H^+/ATP coupling ratio of the ATP synthase from thiol-modulated chloroplasts and two cyanobacterial strains is four. *FEBS Lett.*, **379**, 309–313.

DOI: 10.1093/embo-reports/kve047